Acta Crystallographica Section D
Biological Crystallography
ISSN 0907-4449

Structural and kinetic insights into the mechanism of 5-hydroxyisourate hydrolase from *Klebsiella pneumoniae*

Jarrod B. French and Steven E. Ealick*

Department of Chemistry and Chemical Biology, Cornell University, Ithaca, NY 14853-1301, USA

Correspondence e-mail: see3@cornell.edu

Received 25 March 2011
Accepted 9 May 2011

PDB Reference:
5-hydroxyisourate hydrolase, 3qva.

The stereospecific oxidative degradation of uric acid to (*S*)-allantoin has recently been demonstrated to proceed *via* two unstable intermediates and requires three separate enzymatic reactions. The second step of this reaction, the conversion of 5-hydroxyisourate (HIU) to 2-oxo-4-hydroxy-4-carboxy-5-ureidoimidazoline, is catalyzed by HIU hydrolase (HIUH). The high-resolution crystal structure of HIUH from the opportunistic pathogen *Klebsiella pneumoniae* (KpHIUH) has been determined. KpHIUH is a homotetrameric protein that, based on sequence and structural similarity, belongs to the transthyretin-related protein family. In addition, the steady-state kinetic parameters for this enzyme and four active-site mutants have been measured. These data provide valuable insight into the functional roles of the active-site residues. Based upon the structural and kinetic data, a mechanism is proposed for the KpHIUH-catalyzed reaction.

1. Introduction

The catabolism of uric acid, a key intermediate in the degradation of purines, varies among different organisms. Birds, reptiles, humans and some bacteria lack the necessary enzymes to degrade uric acid (Vogels & Van der Drift, 1976; Zrenner *et al.*, 2006). In humans, the inability to metabolize uric acid can lead to the crystallization of urate in the joints, causing the painful condition known as gout. In many plants and bacteria, however, the high nitrogen content of this molecule makes it an attractive nitrogen source. In all known organisms that catabolize uric acid, a conserved pathway converts this molecule stereospecifically to (*S*)-allantoin (Vogels & Van der Drift, 1976). Until recently, it was believed that a single enzyme, urate oxidase, catalyzed the slow conversion of urate to allantoin. Over the last few years, however, conclusive experiments have been conducted that demonstrate the involvement of two additional enzymes: 5-hydroxyisourate hydrolase (HIUH) and 2-oxo-4-hydroxy-4-carboxy-5-ureidoimidazoline decarboxylase (OHCUD) (Kahn & Tipton, 1997, 1998; Ramazzina *et al.*, 2006). This enzymatic pathway from uric acid to allantoin is shown in Fig. 1.

Klebsiella pneumoniae is an opportunistic human pathogen affecting patients with chronic pulmonary disease and ranks second to *Escherichia coli* as the cause of urinary-tract infections in the elderly (Podschun & Ullmann, 1998). In addition, *K. pneumoniae* is known to cause liver abscesses with metastatic complications (Lederman & Crum, 2005). Two recent genetic studies of *Klebsiella* sp. revealed a cluster of genes that are responsible for the catabolism of uric acid (de la Riva *et al.*,

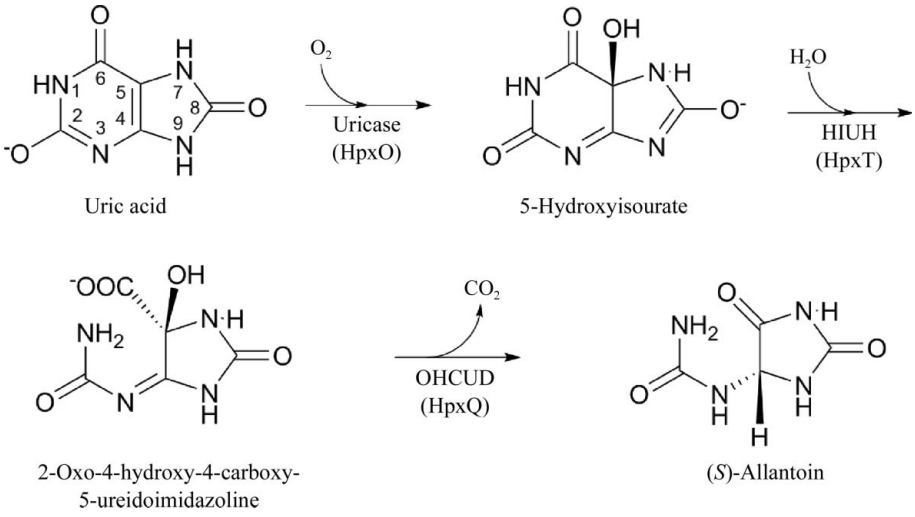

Figure 1
Enzymatic pathway for the conversion of uric acid to allantoin in *K. pneumoniae*.

2008; Pope *et al.*, 2009). Structural and biochemical studies of the proteins encoded by this gene cluster revealed several enzymes with novel functions, including an FAD-dependent urate oxidase and a ureidoglycine aminotransferase (French & Ealick, 2010*a*; O'Leary *et al.*, 2009).

In this work, we report the crystal structure of *K. pneumoniae* HIUH (KpHIUH) at 1.8 Å resolution. In this structure, a phosphate ion occupies the active site and provides clues as to the nature of several important protein–substrate interactions. Guided by the KpHIUH structure, several active-site mutants were constructed and kinetically characterized. These results were used to construct a model of substrate binding and to propose a mechanism of catalysis that is consistent with both the structural and the kinetic data.

2. Materials and methods

2.1. Protein expression and purification

The KpHIUH gene (*hpxT*) was cloned from genomic DNA from *K. pneumoniae* subsp. *pneumoniae* (Schroeter) Trevisan MGH78578 (ATCC 700721) and inserted into a pET-28-based plasmid with an N-terminal His_6 tag. The protein was expressed in BL21 (DE3) cells at 288 K after induction with 0.5 m*M* isopropyl β-D-1-thiogalactopyranoside. KpHIUH was first purified by Ni–NTA (Qiagen) affinity chromatography, which was followed by gel-filtration chromatography on an ÄKTAexplorer FPLC with a HiLoad 26/60 Superdex prep-grade G200 column running 10 m*M* Tris buffer pH 7.6 with 30 m*M* NaCl. After purification, the protein was concentrated to 20 mg ml^{-1} using a centrifugal concentrator and aliquots were flash-frozen and stored at 193 K.

The H7N, R41K, H92N and S108A mutants were made at the Cornell Protein Production and Purification Facility by using site-directed mutagenesis of the native gene. Briefly, site-directed mutagenesis was performed on the KpHIUH gene by a standard PCR protocol using *Pfu*Turbo DNA polymerase (Invitrogen) and *Dpn*I (New England Biolabs) to digest the methylated parental DNA prior to transformation. The presence of the mutated residues was verified by sequencing. The mutant KpHIUH enzymes were expressed and purified in the same manner as the native protein.

2.2. Crystallization, data collection, data processing and structure determination

Crystallization was carried out using the hanging-drop vapor-diffusion method at 291 K. Crystal Screen and Crystal Screen 2 (Hampton Research) and Wizard I and II (Emerald Bio-Systems) sparse-matrix screens were used to identify initial crystallization leads. The protein crystallized well, forming rod-shaped crystals in several of the initial screening conditions. Two of these were optimized and yielded diffraction-quality crystals of similar size and morphology. The optimized conditions included (i) 6–12% PEG 3000, 0.2–0.4 *M* $MgCl_2$ or NaCl and 0.1 *M* cacodylate pH 6.0–6.5 or (ii) 0.5–1.0 *M* ammonium phosphate and 0.1 *M* imidazole pH 7.5–8.5. The rod-shaped crystals were robust and grew over 1–2 weeks. Microseeding of the drops prior to sealing the trays led to crystals of equivalent quality that grew in 2–5 d. The crystals tolerated several different cryoprotection strategies, but were typically cryoprotected in either 30% PEG 3000, 0.2 *M* $MgCl_2$ and 0.1 *M* cacodylate pH 6.0 or 15% glycerol, 15% ethylene glycol, 1.0 *M* ammonium phosphate and 0.1 *M* imidazole pH 7.9. After a brief soak in the cryoprotectant, the crystals were frozen by plunging them into liquid nitrogen and were stored in liquid nitrogen prior to data collection.

Data sets were collected at 100 K on the Northeastern Collaborative Access Team (NE-CAT) beamline 24-ID-E at Argonne National Laboratory (wavelength of 0.979 Å) using a Quantum 315 CCD detector (Area Detector Systems) with 1 s exposure times and 1° oscillations. The data were indexed, integrated and scaled using *HKL*-2000 (Otwinowski & Minor, 1997). The structure was solved by molecular replacement using *MOLREP* (Vagin & Teplyakov, 2010) with an all-alanine version of the structure of *Bacillus subtilis* PucM (PDB entry 2h0e; Jung *et al.*, 2006) as a search model. The model was refined through successive rounds of manual model building using *Coot* (Emsley & Cowtan, 2004) and restrained refinement using *REFMAC*5 (Murshudov *et al.*, 2011). Water molecules were added only after the model converged and this was followed by two additional rounds of refinement. Data-collection and refinement statistics are provided in Table 1.

2.3. Kinetics

All kinetic measurements were carried out in 10 m*M* Tris buffer pH 7.6 containing 30 m*M* NaCl. The substrate for the reaction, 5-hydroxyisourate (HIU), is relatively unstable in

Table 1
Data-collection and refinement statistics.

Values in parentheses are for the highest resolution shell.

Data collection	
Resolution (Å)	1.76
Wavelength (Å)	0.9791
Beamline	APS, 24-ID-C
Space group	$P2_12_12_1$
Unit-cell parameters	
a (Å)	42.19
b (Å)	101.32
c (Å)	106.11
No. of reflections	219892
Unique reflections	45752
Average $I/\sigma(I)$	37.4 (12.3)
Multiplicity	4.8 (4.8)
Completeness (%)	99.4 (100.0)
$R_{\rm merge}$† (%)	4.4 (12.8)
Data refinement	
No. of protein atoms	3177
No. of ligand atoms	20
No. of water atoms	312
Working-set reflections	43252
Test-set reflections	2304
R factor‡	19.8
$R_{\rm free}$§	22.2
R.m.s.d. bonds (Å)	0.01
R.m.s.d. angles (°)	1.17
Mean *B* factor (Å^2)	18.7
Ramachandran plot	
Most favored (%)	100
Additionally allowed (%)	0
Generously allowed (%)	0
Disallowed (%)	0

† $R_{\rm merge} = \sum_{hkl}\sum_i |I_i(hkl) - \langle I(hkl)\rangle|/\sum_{hkl}\sum_i I_i(hkl)$, where $\langle I(hkl)\rangle$ is the mean intensity of *i* reflections with intensities $I_i(hkl)$. ‡ $R = \sum_{hkl}||F_{\rm obs}| - |F_{\rm calc}||/\sum_{hkl}|F_{\rm obs}|$, where $F_{\rm obs}$ and $F_{\rm calc}$ are observed and calculated structure factors, respectively. § For $R_{\rm free}$ the sum extends over a subset of reflections (5%) that were excluded from all stages of refinement.

aqueous solutions and must therefore be generated *in situ* just prior to kinetic analysis. Briefly, an appropriate amount of recombinant uricase from *Candida* sp. (Sigma–Aldrich) was added to a solution of uric acid, resulting in complete conversion to HIU in less than 1 min. The conversion could be monitored by the change in the absorbance spectrum from uric acid to HIU to OHCU (French & Ealick, 2010*b*). Owing to the high rate of turnover of the HIUH enzyme, a stopped-flow instrument (SF-2004, KinTek) was used to measure progress curves for the reaction. Conversion of HIU to OHCU was measured by monitoring the change in absorbance at 293 nm. To calculate kinetic parameters, instantaneous rates at each time, t_x, were approximated by calculating the rate at points along the progress curve using the slope of the line from t_{x-2} to t_{x+2}. These approximate instantaneous rates were plotted against the substrate concentrations and fitted using the Michaelis–Menten equation in order to derive steady-state kinetic parameters (French *et al.*, 2010; Yun & Suelter, 1977). The calculated rate of non-enzymatic hydrolysis of HIU (2.7×10^{-3}) was consistent with a previously reported rate (Kahn & Tipton, 1998) and was taken into account in all rate calculations.

2.4. Modeling of HIU into the KpHIUH active site

The modeling of the ligand in the active site of KpHIUH was performed using v.9.7.211 of *MacroModel* (Mohamadi *et al.*, 1990; http://www.schrodinger.com/products/14/11/). The protein was truncated to a shell containing all atoms within 20 Å of the ligand. Water molecules were removed and the protein-preparation utility was used to add H atoms and to ensure proper ionic states of amino-acid side chains. In order to initially place the substrate, HIU was positioned in the active site by superposition with 8-azaxanthine from the homologous PucM structure (Jung *et al.*, 2006). For the modeling runs, both the active-site residues and the ligand were allowed the freedom to move. The calculations were completed by energy minimization using the AMBER* force field (Weiner *et al.*, 1984) with a distance-dependent dielectric that was further attenuated by a factor of 4. The energy minimization relied upon the TNCG technique (Ponder & Richards, 1987) and was considered to have converged when the energy gradient was less than 0.01 kJ mol^{-1}.

All of the figures presented here were prepared using *PyMOL* (DeLano, 2002) and *ChemBioDraw* (CambridgeSoft). The sequence alignment was generated by *ESPript* (Gouet *et al.*, 2003).

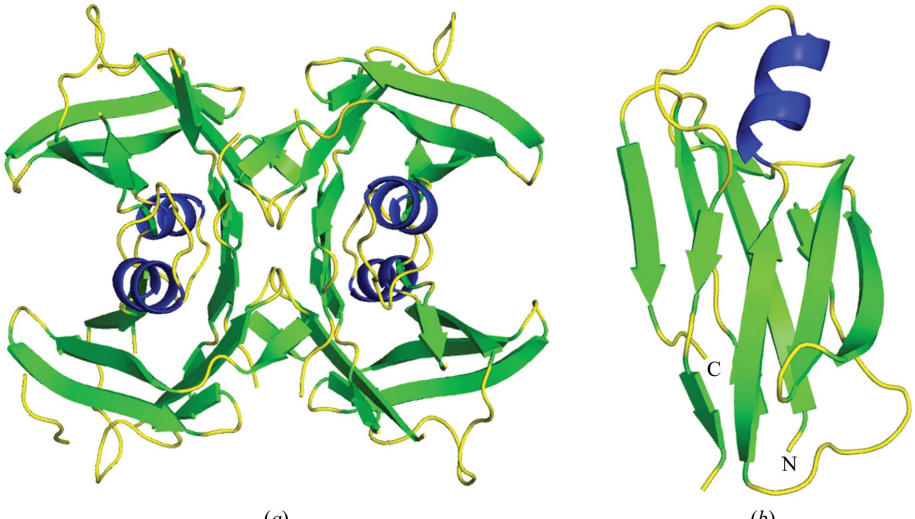

(*a*) (*b*)

Figure 2
Structure of *K. pneumoniae* 5-hydroxyisourate hydrolase. (*a*) KpHIUH tetramer, (*b*) KpHIUH protomer. Helices are colored blue, β-strands are colored green and loop regions are colored yellow. The N- and C-termini are labeled N and C, respectively.

3. Results and discussion

3.1. Overall structure of KpHIUH

KpHIUH crystallized in an orthorhombic space group and contained four protomers in the asymmetric unit. Strong electron density was present for all 108 residues, with the exception of a disordered loop region comprised of residues 84–88. All of the modelled residues have torsion angles consistent

with the most favored region of the Ramachandran plot. The four chains of the enzyme come together to form a homotetramer with 222 symmetry (Fig. 2*a*). Size-exclusion chromatography results are also consistent with a tetrameric species (data not shown). The KpHIUH protomer consists of nine β-strands and one α-helix organized into a β-sandwich structure (Fig. 2*b*). The tetramer is a dimer of dimers, with two protomers arranged to create an extended β-sheet that makes up the dimer–dimer interface. While other HIUH enzymes showed some slight differences in conformation between protomers, there is little structural difference between the chains of KpHIUH [the average root-mean-square deviation (r.m.s.d.) for superposition is 0.28 Å].

3.2. Comparison with other structures

A *BLAST* search (Altschul *et al.*, 1990) using the KpHIUH sequence places this enzyme in the transthyretin-like protein superfamily. This family includes transthyretin, a protein that distributes thyroid hormones throughout the body, and the structurally similar 5-hydroxyisourate hydrolase. All of these proteins are homotetramers that contain an eight-stranded β-sandwich and a small α-helix. The HIUH enzymes are distinguished from transthyretin primarily by the YRGS C-terminal motif. A sequence alignment of KpHIUH, transthyretin and several other transthyretin-like protein family members is shown in Fig. 3(*a*).

A search for structurally related proteins using the *DALI* server (Holm *et al.*, 2008) identified several structural homologs. All of the highly similar structures (Z > 10) were members of the transthyretin-like protein family and included *Salmonella dublin* HIUH (PDB entry 2gpz, r.m.s.d. of 1.1 Å; Hennebry *et al.*, 2006), *E. coli* HIUH (PDB entry 2igl, r.m.s.d. of 1.0 Å; Y. Zuo, J. Blanco, J. Shah, Y. Wang, S. Rivera, T. J. Ragan, G. Hernandez, C. M. Nelersa, R. Mitchell, K. E. Rudd & A. Malhotra, unpublished work), zebrafish HIUH (PDB entry 3iwv, r.m.s.d. of 1.0 Å; Cendron *et al.*, 2011), *B. subtilis* HIUH (PDB entry 2h0e, r.m.s.d. of 1.4 Å; Jung *et al.*, 2006) and several transthyretin structures (rat, PDB entry 1kgj, r.m.s.d. of 1.2 Å; sea bream, PDB entry 1sn0, r.m.s.d. of 1.3 Å; human, PDB entry 1bzd, r.m.s.d. of 1.2 Å; chicken, PDB entry 1tfp, r.m.s.d. of 1.6 Å; Muziol *et al.*, 2001; Eneqvist *et al.*, 2004; Schormann *et al.*, 1998; Sunde *et al.*, 1996). Despite the high degree of similarity to transthyretin (Fig. 3*b*), several recent studies have shown that HIUH enzymes are unable to bind hormones but catalyze the conversion of HIU to OHCU (Hennebry *et al.*, 2006; Kahn & Tipton, 1997, 1998). In addition, the genes for HIUH and OHCUD have been shown to

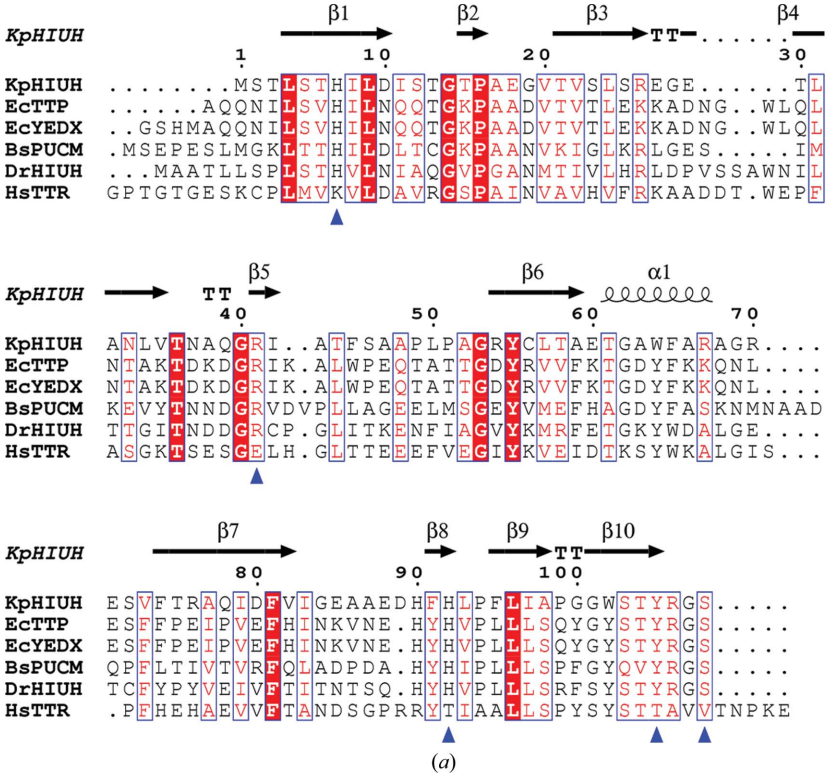

(*a*)

(*b*)

Figure 3
Alignment of KpHIUH with other transthyretin-related proteins (TRPs). (*a*) Sequence alignment of KpHIUH and four other TRPs. The sequences used are those of *K. pneumoniae* HIUH, *E. coli* transthyretin-related protein (EcTTP; PDB entry 2g2n; Lundberg *et al.*, 2006), *E. coli* YedX (EcYEDX; PDB entry 2igl), *B. subtilis* PucM (BsPUCM; PDB entry 2h0e), zebrafish HIUH (DrHIUH; PDB entry 2h1x; Zanotti *et al.*, 2006) and human transthyretin (HsTTR; PDB entry 1f41; Hornberg *et al.*, 2000). In the alignment, residues with red lettering and a blue box are highly conserved, while those with white lettering on a red background are completely conserved. The residues that line the active site of KpHIUH are indicated by blue triangles. The secondary-structure elements shown above the alignment correspond to those observed in the structure of KpHIUH. This figure was generated with *ESPript* (Gouet *et al.*, 2003). (*b*) Structural alignment of KpHIUH (blue) and human transthyretin (green).

Table 2
Kinetic parameters of KpHIUH.

	k_{cat} (s^{-1})	K_m (μM)	k_{cat}/K_m (M^{-1} s^{-1})
Native KpHIUH	172 ± 2	103 ± 2	1.7×10^6
H7N	0.8 ± 0.09	4400 ± 500	1.8×10^2
R41K	34.7 ± 0.4	195 ± 3	1.8×10^5
H92N	0.35 ± 0.01	430 ± 10	8.2×10^2
S108A	81 ± 0.7	93 ± 2	8.7×10^5

appear within clusters of known purine-degradative enzymes (de la Riva *et al.*, 2008; Pope *et al.*, 2009) and are expressed as a single fused gene in several cases (Ramazzina *et al.*, 2006).

3.3. KpHIUH active site

Transthyretin-like proteins are known to possess two active sites per tetramer that are situated at a dimer interface near the surface of the protein. Residues believed to be important for substrate binding and catalysis include the C-terminal tetrapeptide, two histidine residues and an arginine residue from each chain (Fig. 3, blue arrows). These residues and the active-site architecture are also conserved in KpHIUH (Fig. 4*a*). In this structure, a phosphate is seen to be coordinated by the active-site arginine residue (Arg41) and both active-site histidine residues (His7 and His92). This phosphate occupies a position on a plane of noncrystallographic symmetry and appears to bind equally well to both active sites at the dimer interface. To investigate the likely interactions of the active-site residues with the substrate, 5-hydroxyisourate was modeled into the active site. A schematic of the contacts made between the modeled ligand and the active-site residues is shown in Fig. 4(*b*). The positions of the active-site side chains in this model are consistent with those observed in the structure of the *B. subtilis* HIUH complex with 8-azaxanthine and can be used to infer putative roles for the active-site residues. Of the four amino acids of the conserved tetrapeptide sequence, only Tyr105 appears to make significant interactions for binding or catalysis. This residue interacts with the O atom on C8 of the purine ring, most likely to stabilize the charge at this atom and help to orient the HIU molecule for catalysis. Ser108 may also participate in catalysis indirectly by helping to orient and inductively activate His7. The two histidine residues located in the active site, His7 and His92, are situated near the reactive center of the substrate, although only His92 appears to have the correct orientation and distance to form a hydrogen bond to the substrate. The positively charged Arg41 is situated at a hydrogen-bonding distance to the carbonyl at C6 of the purine ring, placing it in an ideal position to stabilize a negative charge at this atom (see mechanistic discussion below).

3.4. Kinetics of native enzyme and active-site mutants

To better understand the different functions that the active-site residues play in catalysis, the kinetic parameters of native KpHIUH and several mutants were characterized. The results (Table 2) are consistent with the structural data and provide additional details about the roles of these residues. Both of the histidine-to-asparagine mutations effectively inactivate the enzyme. Despite the low k_{cat} value, however, the H92N mutant has a K_m that is only fourfold higher than that of the native enzyme. The major difference in k_{cat} values between the native and H92N mutant suggests that His92 plays a direct role in catalysis. The H7N mutant, however, not only experiences a diminished k_{cat} but also has a significantly higher K_m. This indicates that this residue may play a more complicated role in the enzyme mechanism and perhaps participates in substrate binding. An apparent interaction between His7 and the hydroxyl group of HIU (Fig. 4*b*) would explain a possible role in orienting the substrate for catalysis. The S108A mutation does not substantially alter the K_m and leads to only a twofold reduction in rate, implying that Ser108 is not likely to

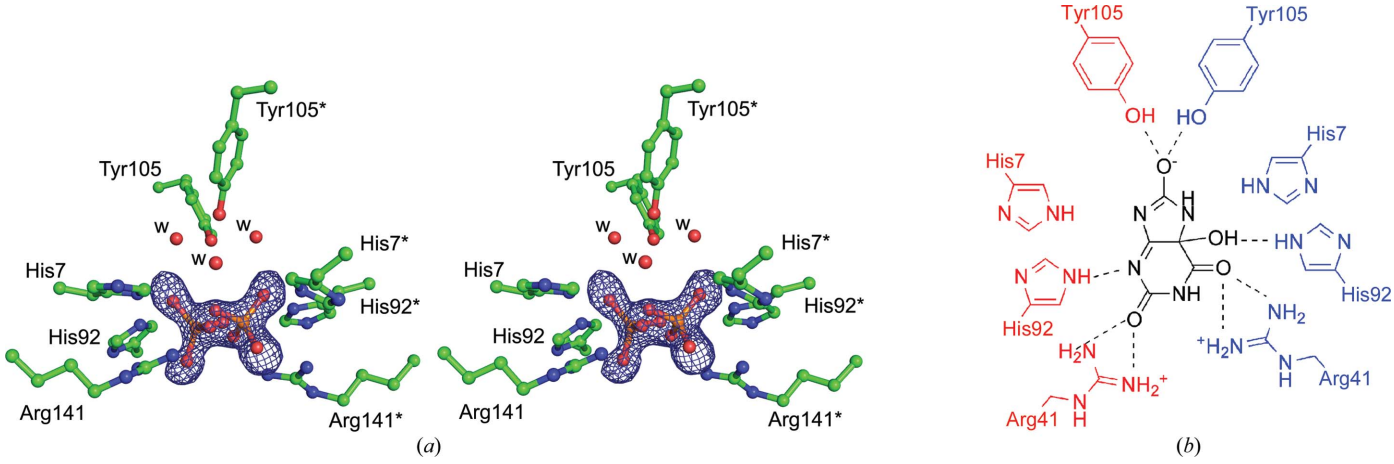

Figure 4
KpHIUH active site. (*a*) A stereodiagram of the active site of the KpHIUH–phosphate complex is shown. Residue names followed by an asterisk (*) are from the adjoining chain. In this figure C atoms are colored green, O atoms are colored red, N atoms are colored blue, P atoms are colored orange and water atoms are shown as red spheres and labeled with a 'w'. The electron density shown is from an $F_o - F_o$ map contoured at 3σ that was calculated before adding the phosphate. Note that as the active site coincides with a noncrystallographic symmetry plane, the phosphate molecule is modeled in two alternative orientations. (*b*) A schematic of 5-hydroxyisourate modeled into the active site of KpHIUH. Residues from the two different chains are colored red and blue, while the ligand is shown in black.

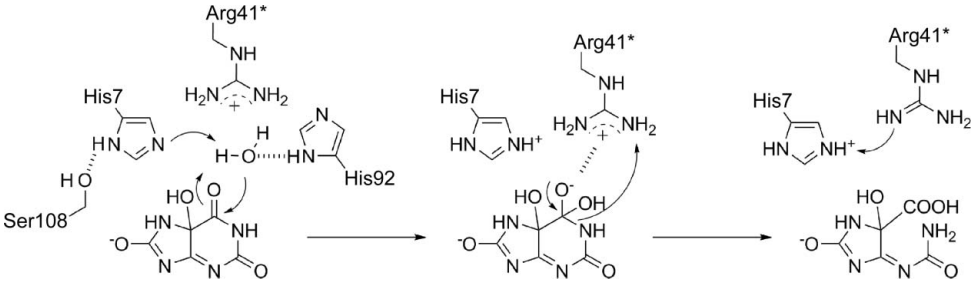

Figure 5
A mechanistic proposal for the conversion of 5-hydroxyisourate to 2-oxo-4-hydroxy-4-carboxy-5-ureidoimidazoline by *K. pneumoniae* HIUH.

participate in binding or catalysis. Similarly, the R41K mutant retains much of its activity, but the fivefold decrease in rate and twofold increase in K_m suggest some minor role in the reaction mechanism. As suggested by the structure, it is likely that Arg41 primarily interacts with the C6 carbonyl O atom, hydrogen bonding to the substrate and possibly helping to stabilize a negative charge at this atom during the reaction.

3.5. Proposed mechanism of KpHIUH

A mechanism for the HIUH reaction was first proposed by Tipton and coworkers for the soybean (*Glycine max*) enzyme and was based primarily upon structural alignments with proteins of known function and kinetic data from site-directed mutants (Raychaudhuri & Tipton, 2003; Sarma *et al.*, 1999). In this mechanism an active-site glutamate is implicated as the nucleophile that initiates the reaction. This protein, however, belongs to the type I glycosidase family and is not structurally homologous to the transthyretin-like HIUH enzymes. The transthyretin-like HIUH enzymes not only lack such a glutamate residue but do not possess any strong nucleophile in their active sites.

Based upon the structural and kinetic data for KpHIUH, a mechanistic proposal for the transthyretin-like HIUH is presented in Fig. 5. Owing to the lack of a strong nucleophile in the active site, the reaction is likely to be initiated by a water molecule that is first activated by deprotonation. Considering the geometry of the two histidine residues in the active site as well as the kinetic data, it is likely that both of these residues take part in this deprotonation step. The hydrogen-bonding interactions between the water molecule and the two histidine residues, His7 and His92, would serve to orient the water ideally for attack at C6 of the purine ring. The highly conserved C-terminal serine residue, Ser108 in KpHIUH, is in position to form a hydrogen bond to His7 and may indirectly participate in catalysis by inductively activating this residue. Deprotonation of the water by His7 creates a hydroxide nucleophile that attacks C6 of the purine ring, leading to a tetrahedral oxyanion intermediate. The charge on the resulting oxyanion would be stabilized by the positively charged guanidinium group of Arg41. It is clear from the direction of the attack and the geometry of the resulting tetrahedral center that Arg41 from the neighboring chain helps to stabilize the charge on the oxyanion intermediate. Collapse of the oxyanion would then lead to ring opening, with the final proton coming from the nearby Arg41. The original proton abstracted from a water molecule by His7 would then be transferred to Arg41 to complete the catalytic cycle.

The crystal structure and kinetic analysis of KpHIUH presented here provide important details about the mechanism of this enzyme and the roles that the active-site residues play during substrate binding and catalysis. These results move us a step closer to complete characterization of the enzymes involved in the purine catabolic pathway in the opportunistic human pathogen *K. pneumoniae*. In addition, this structure, together with others involved in the pathway, helps to suggest potential targets for antimicrobial therapies that target purine metabolism in this organism.

This work was supported by NIH grant GM73220. We would like to thank the staff at NE-CAT for advice with data collection and processing. Data collected at the Northeastern Collaborative Access Team beamlines of the Advanced Photon Source are supported by award RR-15301 from the National Center for Research Resources at the National Institutes of Health. Use of the Advanced Photon Source is supported by the US Department of Energy, Office of Basic Energy Sciences under Contract No. DE-AC02-06CH11357. We would like to acknowledge Cynthia Kinsland of the Protein Production Facility in the Department of Chemistry and Chemical Biology for help with molecular biology and Leslie Kinsland for help with manuscript preparation. JBF would like to acknowledge the Tri-Institutional Training Program in Chemical Biology for financial support.

References

Altschul, S. F., Gish, W., Miller, W., Myers, E. W. & Lipman, D. J. (1990). *J. Mol. Biol.* **215**, 403–410.
Cendron, L., Ramazzina, I., Percudani, R., Rasore, C., Zanotti, G. & Berni, R. (2011). *J. Mol. Biol.*, doi:10.1016/j.jmb.2011.04.022.
DeLano, W. L. (2002). *PyMOL*. http://www.pymol.org.
Emsley, P. & Cowtan, K. (2004). *Acta Cryst.* D**60**, 2126–2132.
Eneqvist, T., Lundberg, E., Karlsson, A., Huang, S., Santos, C. R., Power, D. M. & Sauer-Eriksson, A. E. (2004). *J. Biol. Chem.* **279**, 26411–26416.
French, J. B., Cen, Y., Vrablik, T. L., Xu, P., Allen, E., Hanna-Rose, W. & Sauve, A. A. (2010). *Biochemistry*, **49**, 10421–10439.
French, J. B. & Ealick, S. E. (2010*a*). *Biochemistry*, **49**, 5975–5977.
French, J. B. & Ealick, S. E. (2010*b*). *J. Biol. Chem.* **285**, 35446–35454.
Gouet, P., Robert, X. & Courcelle, E. (2003). *Nucleic Acids Res.* **31**, 3320–3323.
Hennebry, S. C., Wright, H. M., Likic, V. A. & Richardson, S. J. (2006). *Proteins*, **64**, 1024–1045.
Holm, L., Kääriäinen, S., Rosenström, P. & Schenkel, A. (2008). *Bioinformatics*, **24**, 2780–2781.
Hornberg, A., Eneqvist, T., Olofsson, A., Lundgren, E. & Sauer-Eriksson, A. E. (2000). *J. Mol. Biol.* **302**, 649–669.

Jung, D.-K., Lee, Y., Park, S. G., Park, B. C., Kim, G.-H. & Rhee, S. (2006). *Proc. Natl Acad. Sci. USA*, **103**, 9790–9795.
Kahn, K. & Tipton, P. A. (1997). *Biochemistry*, **36**, 4731–4738.
Kahn, K. & Tipton, P. A. (1998). *Biochemistry*, **37**, 11651–11659.
Lederman, E. R. & Crum, N. F. (2005). *Am. J. Gastroenterol.* **100**, 322–331.
Lundberg, E., Bäckström, S., Sauer, U. H. & Sauer-Eriksson, A. E. (2006). *J. Struct. Biol.* **155**, 445–457.
Mohamadi, F., Richards, N. G. J., Guida, W. C., Liskamp, R., Lipton, M., Caufield, C., Chang, G., Hendrickson, T. & Still, W. C. (1990). *J. Comput. Chem.* **11**, 440–467.
Murshudov, G. N., Skubák, P., Lebedev, A. A., Pannu, N. S., Steiner, R. A., Nicholls, R. A., Winn, M. D., Long, F. & Vagin, A. A. (2011). *Acta Cryst.* D**67**, 355–367.
Muziol, T., Cody, V. & Wojtczak, A. (2001). *Acta Biochim. Pol.* **48**, 885–892.
O'Leary, S. E., Hicks, K. A., Ealick, S. E. & Begley, T. P. (2009). *Biochemistry*, **48**, 3033–3035.
Otwinowski, Z. & Minor, W. (1997). *Methods Enzymol.* **276**, 307–326.
Podschun, R. & Ullmann, U. (1998). *Clin. Microbiol. Rev.* **11**, 589–603.
Ponder, J. W. & Richards, F. M. (1987). *J. Comput. Chem.* **8**, 1016–1024.
Pope, S. D., Chen, L.-L. & Stewart, V. (2009). *J. Bacteriol.* **191**, 1006–1017.
Ramazzina, I., Folli, C., Secchi, A., Berni, R. & Percudani, R. (2006). *Nature Chem. Biol.* **2**, 144–148.
Raychaudhuri, A. & Tipton, P. A. (2003). *Biochemistry*, **42**, 6848–6852.
Riva, L. de la, Badia, J., Aguilar, J., Bender, R. A. & Baldoma, L. (2008). *J. Bacteriol.* **190**, 7892–7903.
Sarma, A. D., Serfozo, P., Kahn, K. & Tipton, P. A. (1999). *J. Biol. Chem.* **274**, 33863–33865.
Schormann, N., Murrell, J. R. & Benson, M. D. (1998). *Amyloid*, **5**, 175–187.
Sunde, M., Richardson, S. J., Chang, L., Pettersson, T. M., Schreiber, G. & Blake, C. C. (1996). *Eur. J. Biochem.* **236**, 491–499.
Vagin, A. & Teplyakov, A. (2010). *Acta Cryst.* D**66**, 22–25.
Vogels, G. D. & Van der Drift, C. (1976). *Bacteriol. Rev.* **40**, 403–468.
Weiner, S. J., Kollman, P. A., Case, D. A., Singh, U. C., Ghio, C., Alagona, G., Profeta, S. Jr & Weiner, P. (1984). *J. Am. Chem. Soc.* **106**, 765–784.
Yun, S.-L. & Suelter, C. H. (1977). *Biochim. Biophys. Acta*, **480**, 1–13.
Zanotti, G., Cendron, L., Ramazzina, I., Folli, C., Percudani, R. & Berni, R. (2006). *J. Mol. Biol.* **363**, 1–9.
Zrenner, R., Stitt, M., Sonnewald, U. & Boldt, R. (2006). *Annu. Rev. Plant Biol.* **57**, 805–836.